Chemical Geology 284 (2011) 296–305

Contents lists available at ScienceDirect

Chemical Geology

journal homepage: www.elsevier.com/locate/chemgeo

Research papers

Vibrational, X-ray absorption, and Mössbauer spectra of sulfate minerals from the weathered massive sulfide deposit at Iron Mountain, California

Juraj Majzlan [a,*], Charles N. Alpers [b], Christian Bender Koch [c], R. Blaine McCleskey [d], Satish C.B. Myneni [e], John M. Neil [f]

[a] Institute of Geosciences, Friedrich-Schiller-University, Burgweg 11, Jena, D-07749, Germany
[b] U.S. Geological Survey, 6000 J Street, Placer Hall, Sacramento CA 95819, USA
[c] Department of Basic Sciences and Environment, University of Copenhagen, Thorvaldsensvej 40, DK-1871 Frederiksberg C, Denmark
[d] U.S. Geological Survey, 3215 Marine Street, Suite E-127, Boulder CO 80303, USA
[e] Department of Geosciences, Princeton University, Princeton NJ 08544, USA
[f] Thermochemistry Facility, Department of Chemical Engineering and Materials Science, University of California, Davis CA 95616, USA

ARTICLE INFO

Article history:
Received 28 September 2010
Received in revised form 28 February 2011
Accepted 10 March 2011
Available online 17 March 2011

Editor: D.B. Dingwell

Keywords:
Iron Mountain
Sulfate minerals
Infrared spectra
X-ray absorption spectra
Mössbauer spectra
Oxygen bridging

ABSTRACT

The Iron Mountain Mine Superfund site in California is a prime example of an acid mine drainage (AMD) system with well developed assemblages of sulfate minerals typical for such settings. Here we present and discuss the vibrational (infrared), X-ray absorption, and Mössbauer spectra of a number of these phases, augmented by spectra of a few synthetic sulfates related to the AMD phases. The minerals and related phases studied in this work are (in order of increasing Fe_2O_3/FeO): szomolnokite, rozenite, siderotil, halotrichite, römerite, voltaite, copiapite, monoclinic $Fe_2(SO_4)_3$, $Fe_2(SO_4)_3 \cdot 5H_2O$, kornelite, coquimbite, Fe(SO_4)(OH), jarosite and rhomboclase. Fourier transform infrared spectra in the region 750–4000 cm^{-1} are presented for all studied phases. Position of the FTIR bands is discussed in terms of the vibrations of sulfate ions, hydroxyl groups, and water molecules. Sulfur K-edge X-ray absorption near-edge structure (XANES) spectra were collected for selected samples. The feature of greatest interest is a series of weak pre-edge peaks whose position is determined by the number of bridging oxygen atoms between Fe^{3+} octahedra and sulfate tetrahedra. Mössbauer spectra of selected samples were obtained at room temperature and 80 K for ferric minerals jarosite and rhomboclase and mixed ferric–ferrous minerals römerite, voltaite, and copiapite. Values of $Fe^{2+}/[Fe^{2+} + Fe^{3+}]$ determined by Mössbauer spectroscopy agree well with those determined by wet chemical analysis. The data presented here can be used as standards in spectroscopic work where spectra of well-characterized compounds are required to identify complex mixtures of minerals and related phases.

1. Introduction

Iron sulfates compose a large and variable group of minerals that are most commonly linked to acid mine or acid rock drainage, i.e., discharge of acidic waters produced by weathering of sulfides in ore, mine waste, or undisturbed geological materials. Acidic discharges are generally rich in iron, aluminum, heavy metals, and sulfate ions and commonly precipitate sulfate minerals in association with evaporation and microbial oxidation of ferrous iron (Nordstrom and Alpers, 1999; Jambor et al., 2000). Acid mine drainage (AMD) is a widely recognized environmental problem because of the acidification of soils, streams, and underground water. This problem can present a threat to living organisms, including humans (Nordstrom et al., 2000; Buckby et al., 2003). One of the best and well-studied examples of an AMD system is the Iron Mountain Mines Superfund site in California, USA (e.g., Alpers et al., 2003). Here, a large number of sulfate minerals precipitate because the acidity reaches formidable levels (Nordstrom et al., 2000) and the concentration of the dissolved solutes is prodigious. Macroscopic samples of the sulfate minerals lend themselves not only for the detailed mineralogical and geochemical studies (Nordstrom and Alpers, 1999; Nordstrom et al., 2000) but are also excellent for the collection of various types of spectra because of the relative ease of separation and characterization of such material.

The sequence of iron-sulfate and iron-oxide mineral precipitates follows specific spatial patterns that may guide remediation efforts if these patterns are recognized. Field identification can be based on visual inspection, or more efficiently, by aerial mapping using reflected IR and visible light radiation (e.g., Hunt (1979); Townsend (1987); Swayze et al. (2000); Montero-Sanchez et al. (2005)). In addition, there is considerable interest in mapping the distribution

* Corresponding author at: Friedrich-Schiller University, Institute of Geosciences, Burgweg 11, D-07749 Jena, Germany. Tel.: +49 3641 948700; fax: +49 3641 948602.
E-mail address: Juraj.Majzlan@uni-jena.de (J. Majzlan).

0009-2541/$ – see front matter © 2011 Elsevier B.V. All rights reserved.
doi:10.1016/j.chemgeo.2011.03.008

of sulfate minerals on extra-terrestrial targets using remote sensing (e.g., Vilas et al. (1994); Geissler et al. (1993); Klingelhöfer et al. (2004); Morris et al. (2004); Gendrin et al. (2005); Langevin et al. (2005)).

In a laboratory, more quantitative techniques, such as X-ray powder diffraction (XRD) or Fourier transform infrared (FTIR) spectroscopy may be utilized. Powder patterns of most natural iron-sulfate minerals are tabulated (ICDD Powder Diffraction Files), and XRD techniques may be used routinely on these samples. On the other hand, exhaustive spectroscopic information that could find their use in laboratory studies, aerial mapping, and extra-terrestrial remote sensing is generally not available. The iron-sulfate minerals could be used for further understanding of megascopic and macroscopic features on Earth and also on other bodies in the solar system.

Iron sulfates can provide valuable insight into microscopic phenomena, such as magnetic frustration (Wills and Harrison, 1996), redox conditions of geochemical systems, or interaction of iron and sulfate at interfaces and in solutions (Majzlan and Myneni, 2005). A plethora of spectroscopic techniques may be applied to these compounds to gather the necessary information. In many cases, the spectra, which may serve as a starting or reference point, have not been reported.

The goal of this study is to expand the existing data sets with FTIR, XANES, and Mössbauer spectra taken on a suite of sulfate minerals and phases that may be found in AMD systems. The samples were all characterized by X-ray diffraction and wet chemical analyses to provide the basic structural and chemical data. In this work, we provide only a brief explanation of the observed spectral features even though the results of each of the techniques for each of the minerals deserve much more detailed attention. In specific cases, we are currently working on the interpretation of such details and the results will be reported separately. The database presented here should be regarded as a reference from which a particular mineral can be selected as an appropriate representative of an unknown in a specific study.

2. Materials and methods

Both natural and synthetic samples were used in this study. Natural samples were collected at the Iron Mountain Mine Superfund site, California (Fig. 1) (Nordstrom and Alpers, 1999; Nordstrom et al., 2000; Alpers et al., 2003). The fewer synthetic samples were prepared according to the procedures described by Posnjak and Merwin (1922). The exception was monoclinic $Fe_2(SO_4)_3$ which was prepared according to the procedure described by Long et al. (1979).

X-ray diffraction patterns were collected with a Scintag PAD V diffractometer, Cu Kα radiation and a diffracted beam graphite monochromator. The starting crystal structure models were refined by the Rietveld technique using GSAS (Larson and von Dreele, 1994).

Metal concentrations in the ferric sulfate samples were determined by inductively-coupled plasma optical-emission spectrometry (ICP-OES). The samples were also analyzed by the Ferrozine method for Fe^{2+} (Stookey, 1970), and Fe^{3+} was determined by the difference between total Fe and Fe^{2+}. Sulfate concentrations were analyzed by ion chromatography.

The infrared spectra were collected with a Bruker Fourier transform infrared (FTIR) spectrometer with a DTGS (deuterated triglycine sulfate) detector and a KBr beamsplitter. The spectral resolution was 4 cm^{-1} and the spectra were measured from 750 to 4000 cm^{-1}. Most samples were embedded in a KCl pellet and analyzed in the transmission mode. Some samples, especially rhomboclase, were found to react rapidly with KBr or KCl, and the spectra could be collected only in attenuated total reflectance (ATR) mode with samples pressed against a single-reflection diamond crystal. The rhomboclase sample had to be carefully dried before data collection because the solution

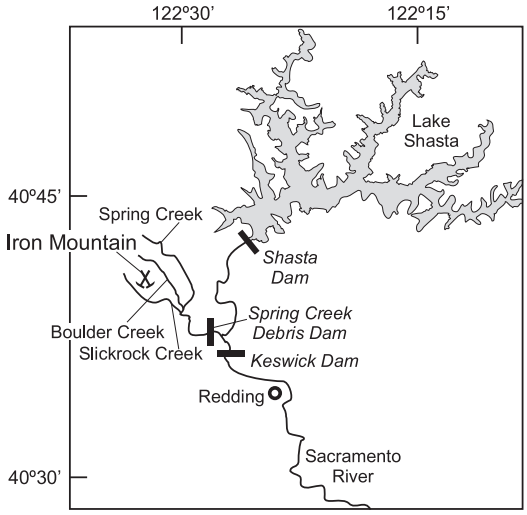

Fig. 1. Location of Iron Mountain mine in northern California, near the city of Redding.

associated with rhomboclase (concentrated H_2SO_4) could damage the diamond crystal.

XANES spectra were collected at the Stanford Synchrotron Radiation Lightsource (SSRL) using beamline 6–2 and Si (111) monochromator crystals. The incident photon flux was enhanced with a He-flight path chamber. The spectra were collected in the fluorescence mode using a Lytle detector. All of the sulfate spectra were calibrated against the low-energy transition in solid $Na_2(SO_3S)\cdot 5H_2O$, which was set at 2469.2 eV. The spectra of $Na_2(SO_3S)\cdot 5H_2O$ were collected frequently during the XANES data measurements to correct for the systematic error associated with the drift of the monochromator.

Mössbauer spectra were obtained at room temperature and 80 K using a conventional constant acceleration spectrometer with a ^{57}Co in Rh source. The spectrometer was calibrated using a 12.5 μm foil of natural Fe at room temperature and isomer shifts are given with respect to the center of the spectrum of this sample. The samples were transferred into self-supporting Perspex holders and their amounts were adjusted to ensure that the maximum absorption of any component was smaller than 6%. Fitting of the paramagnetic spectra were carried out using simple Lorentzian shaped doublets that was carried to have identical linewidths in complex spectra. The experimental line width of the instrumental setup is 0.22 mms^{-1}.

3. Crystal structures

Crystal structures of sulfate minerals were reviewed by Hawthorne et al. (2000) so we will only briefly discuss the structural features important in the evaluation of this work. The crystal structures considered are built by SO_4 tetrahedra, $Fe(O,OH,H_2O)_6$ octahedra, hydroxyl groups or water molecules. The connectivity of the octahedral and tetrahedral units is briefly described and depicted in Table 1. With the exception of network structures (e.g., szomolnokite), the octahedral–tetrahedral units (clusters, chains, or sheets) are held together by a network of hydrogen bonds. The position of hydrogen atoms in these structures is generally not known or poorly known. Some structures (e.g., copiapite) contain water molecules that link the structural units. The presence of the H_3O^+ ion in hydronium jarosite or alunite has been suspected (Ripmeester et al., 1986; Wills and Harrison, 1996) and definitely proven by NMR studies (Nielsen et al., 2008). The intersheet portion in rhomboclase is believed to contain $(H_5O_2)^+$ groups (Mereiter, 1974). At least one proton is mobile at room temperature as indicated by proton conductivity studies (Brach and Goodenough, 1988).

Table 1
The studied phases, their nominal composition, and site symmetries for the sulfur and iron cations. Site symmetries for sulfur and iron sites can aid in the interpretation of FTIR and Mössbauer spectra, respectively. Fragments of several structures of the studied minerals are shown and display the connectivity of iron octahedra and sulfate tetrahedra. The arrangement of the polyhedra can be used in explanation of the XANES spectra.

Mineral nominal composition	Sulfur site symmetry sketch of the structure (see also text)	Iron site symmetry	Brief description of the structure (reference for the initial model used in Rietveld refinement)
Jarosite $KFe_3(SO_4)_2(OH)_6$ Hydronium jarosite $(H_3O)Fe_3(SO_4)_2(OH)_6$	C_{3v} 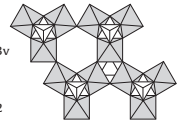	C_{2h}	Octahedral sheets decorated by sulfate tetrahedra (Hendricks, 1937)
Szomolnokite $Fe^{2+}SO_4 \cdot H_2O$	C_2	C_i	Network structure; octahedral chains are interlinked by sulfate tetrahedra (le Fur et al., 1966)
Rozenite $Fe^{2+}SO_4 \cdot 4H_2O$	C_1	C_1	Clusters of two octahedra and two tetrahedra (Baur, 1962)
Siderotil $Fe^{2+}SO_4 \cdot 5H_2O$	C_1	C_i, C_i	Chains of alternating octahedra and tetrahedra (Peterson et al., 2003)
Monoclinic $Fe_2^{3+}(SO_4)_3$	C_1, C_1, C_1	C_1, C_1	Network structure; octahedra and tetrahedra alternate in directions (Long et al., 1979)
$Fe_2^{3+}(SO_4)_3 \cdot 5H_2O$	C_1, C_1, C_1	C_1, C_1	Corrugated slabs where iron octahedra are interlinkcd by sulfate tetrahedra (Majzlan et al., 2005)
Kornelite $Fe_2^{3+}(SO_4)_3 \cdot 7.25H_2O$	C_1, C_1, C_1	C_1, C_1	Sheets built by alternating octahedra and tetrahedra (Robinson and Fang, 1973)
Coquimbite $Fe^{2+}(SO_4)_3 \cdot 9H_2O$	C_1 	D_3, C_3	Clusters of three iron octahedra and four sulfate tetrahedra; isolated octahedra (Fang and Robinson, 1970)
Copiapite $Fe^{2+}Fe_4^{3+}(SO_4)_6(OH)_2 \cdot 20H_2O$ Ferricopiapite $Fe_{14/3}^{3+}(SO_4)_6(OH)_2 \cdot 20H_2O$	C_1, C_1, C_1 	C_i, C_1, C_1 (Fe^{2+}, if present, on C_i)	Chains in which two octahedra alternate with a sulfate tetrahedron; isolated octahedra (Fanfani et al., 1973)
$Fe^{3+}(SO_4)(OH)$	C_s	C_s	Network structure; octahedral chains are interlinked by sulfate tetrahedra (Johansson, 1962)
Voltaite $K_2Fe_5^{2+}Fe_4^{3+}(SO_4)_{12} \cdot 18H_2O$	C_1	Fe^{3+}: C_{3i} Fe^{2+},Fe^{3+}: C_2	Framework structure; $Fe^{3+}O_6$. octahedra share six corners with six sulfate tetrahedra; these $(Fe^{3+}O_6(SO_4)_6$ pinwheels are connected to $[Fe_{5/6}^{2+}Fe_{1/6}^{3+}O_4(H_2O)_2]$ octahedra and KO_{12} polyhedra (Mereiter, 1972)
Halotrichite $Fe^{2+}Al_2(SO_4)_4 \cdot 22H_2O$	C_1, C_1, C_1, C_1	C_1	Isolated $Al(H_2O)_6$ octahedra; clusters of Fe^{2+} octahedron and sulfate tetrahedron (Quartieri et al., 2000)
Römerite $Fe^{2+}Fe_2^{3+}(SO_4)_4 \cdot 14H_2O$	C_1, C_1 	Fe^{2+}: $C_i$$Fe^{3+}$: C_1	Fe^{2+} in isolated octahedra; Fe^{3+} octahedron forms a cluster with two sulfate tetrahedra (Fanfani et al., 1970)
Rhomboclase $(H_3O)Fe^{3+}(SO_4)_4 \cdot 3H_2O$	C_1 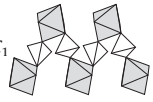	C_1	Sheets built by alternating octahedra (Mereiter, 1974)

4. Results and discussion

4.1. Chemical and structural data

The phases used in this study were identified by their macroscopic physical properties, parameters derived from XRD patterns (Table 2), and chemical analyses (Table 3). Samples were not analyzed for water content, therefore, the nominal water content is assumed. The starting models for Rietveld refinement were taken from references given in Table 1. With the exception of the sample IM-05, all the studied samples were unambiguously identified by XRD and chemical analysis.

The sample IM-05 was collected and identified in the field as copiapite. The identification was confirmed by chemical analysis (Table 3) and all the applied spectroscopic techniques. The XRD pattern shows sharp peaks, including the peak diagnostic for copiapite-group minerals at $d = 18.26$ Å. The pattern was indexed by a LeBail fit (see Table 2) based on the data of similar Zn- and Ni-compounds synthesized and studied by Majzlan and Michallik (2007). The crystal structure of these phases is not known. It can be assumed, however, that it is a structure closely related to that of copiapite (cf. Majzlan and Michallik (2007)).

4.2. Infrared spectroscopy

Infrared spectroscopy probes vibrational transitions associated with a change in dipole moment in the molecule or crystal structure (Harris and Bertolucci, 1978). Within the spectral region covered in this study (Figs. 2 and 3), such transitions include the stretching and bending modes of O—H and H—O—H bonds, and stretching vibrations of the SO_4 group. Vibrations involving bending of the SO_4 groups and the $Fe(O,OH,OH_2)_6$ octahedral units occur at lower frequencies, and are unlikely to appear in these spectra.

The stretching O—H vibrations (νOH) in simple hydroxides of Fe and Al occur at 2900–3660 cm^{-1} and M—O—H bending vibrations (δOH) at 900–1170 cm^{-1} (Ryskin, 1974). The O—H vibrations in the studied sulfates can be expected to have frequencies in the same range. Water in the gaseous state has three modes at 3657 ($\nu_1 w$), 3756 ($\nu_3 w$), and 1595 ($\nu_2 w$) cm^{-1} (Ryskin, 1974). The $\nu_2 w$ mode is therefore indicative of H—O—H bending vibration because it does not overlap with any O—H vibration. This vibration may originate in H_2O molecule as well as $(H_3O)^+$ and $(H_5O_2)^+$ ions.

An undistorted SO_4 group with tetrahedral symmetry has four modes of vibration (Table 4). Of these, only two modes fall in the spectral range of this study. The frequencies of these modes are 1102 and 981 cm^{-1}. The former is an asymmetric stretching, triply degenerate, IR-active band designated ν_3SO_4; the latter is a symmetric stretching, non-degenerate, Raman-active band designated ν_1SO_4. If the symmetry of the SO_4 group is lowered, the degeneracy of the ν_3SO_4 mode is lifted and the mode inactive in tetrahedral symmetry (ν_1SO_4) becomes IR active. Therefore, each crystallographically distinct sulfate contributes 1 (single ν_3) to 4 (three ν_3 and one ν_1) bands to these spectra depending on the site symmetry at the sulfur

Table 2
Space groups and lattice parameters of the studied samples.

Phase, sample ID	Space group	Lattice parameters (Å, °)
Natural samples		
Szomolnokite, IM-01	$C2_1/c$	a = 7.0764(6), b = 7.5480(6), c = 7.6002(6), β = 116.176(4)
Rhomboclase, IM-02	*Pnma*	a = 9.726(3), b = 18.293(9), c = 5.428(3)
IM-05[a]	Triclinic	a = 7.3820(1), b = 7.3831(1), c = 36.614(1) α = 92.919(2), β = 92.911(2), γ = 102.413(1)
Copiapite, 91RS 210A	$P\bar{1}$	a = 7.3453(2), b = 18.7332(8), c = 7.3675(3) α = 91.448(3), β = 102.188(3), γ = 99.067(3)
Voltaite, IMJ-05	$Fd\bar{3}c$	a = 27.206(2)
Voltaite, IM-06	$Fd\bar{3}c$	a = 27.214(2)
Voltaite, IMJ-06	$Fd\bar{3}c$	a = 27.204(2)
Voltaite, 91RS 210A	$Fd\bar{3}c$	a = 27.232(2)
Kornelite, IM-09	$P2_1/n$	a = 14.319(5), b = 20.139(6), c = 5.429(2), β = 96.78(2)
Jarosite, IMJ-09	$R\bar{3}m$	a = 7.315(1), c = 17.179(5)
Römerite, IM-10	$P\bar{1}$	a = 6.453(1), b = 15.309(3), c = 6.322(1) α = 90.146(8), β = 100.932(9), γ = 85.86(1)
Halotrichite, IM-11	$P2_1/c$	a = 6.184(1), b = 24.276(6), c = 21.237(4), β = 100.46(1)
Coquimbite, IM-12	$P\bar{3}1c$	a = 10.9153(4), c = 17.0770(8)
Rozenite, IM-13	$P2_1/n$	a = 5.9638(5), b = 13.607(1), c = 7.9618(6), β = 90.482(6)
Siderotil, IM-14	$P\bar{1}$	a = 6.294(2), b = 10.638(3), c = 6.070(2) α = 82.22(2), β = 109.83(2), γ = 105.10(2)
Synthetic samples		
Ferricopiapite	$P\bar{1}$	a = 7.3867(6), b = 18.363(2), c = 7.3275(5) α = 93.940(5), β = 102.201(5), γ = 98.916(4)
$Fe_2(SO_4)_3$	$P2_1/n$	a = 8.2957(7), b = 8.5358(8), c = 11.625(1), β = 90.729(6)
$Fe_2(SO_4)_3 \cdot 5H_2O$	$P2_1/m$	a = 10.705(1), b = 11.080(1), c = 5.5736(6), β = 98.864(6)
Hydronium jarosite	$R\bar{3}m$	a = 7.35463(2), c = 17.01795(4)
$Fe(OH)(SO_4)$	*Pnma*	a = 7.333(1), b = 6.415(1), c = 7.138(1)
Rhomboclase	*Pnma*	a = 9.7226(8), b = 18.2800(9), c = 5.4270(5)

[a] The structure of this phase is not known but is most likely closely related to that of copiapite (see text for details). The lattice parameters were refined in a LeBail fit.

positions (Table 1). The symmetry apparent from the spectra depends on the degree of distortion of the SO_4 group. Even if the symmetry of SO_4 group is lower than T_d, the splitting may be too small and become obscured by overlap of the individual sulfate bands. The problem is further compounded by possible overlap of the S—O stretching and O—H bending vibrations.

IR data for numerous sulfates and other salts with tetrahedral oxyanions were reviewed by Farmer (1974). A newer dataset for a number of sulfate minerals was presented by Dyar et al. (2005).

There are additional weak bands in our spectra (Fig. 3). Organic impurities in our natural samples of kornelite and romerite are the cause of the appearance of a triplet with a peak at 2922 cm^{-1}, characteristic of the C—H stretching vibrations. The weak bands at ~1450 cm^{-1} are due to the C—H bending vibrations.

4.2.1. Ferrous sulfate hydrates

There should be four sulfate bands in the spectra of each $FeSO_4 \cdot nH_2O$ compound due to a relatively low sulfur site symmetry

Table 3
Chemical composition of the sulfate samples. Note that not all samples were analyzed, although lattice parameters are reported for all. The formulae were calculated from the wet-chemical analyses. Small charge imbalances in the formulae are caused by analytical errors.

Phase, sample ID	$Fe^{2+}/(Fe^{2+}+Fe^{3+})$		
Formula based on chemical analysis	Ideal	Analytical[a]	Analytical[b]
Natural samples			
Szomolnokite, IM-01: $(Fe_{0.88}Zn_{0.06}Ca_{0.01})^{2+}SO_4 \cdot H_2O$	1.00	1.00	
Rhomboclase, IM-02: $(H_3O)Fe^{3+}(SO_4)_2 \cdot 3H_2O$	0.00	0.00	0.00
IM-05: $(Fe_{0.54}Zn_{0.38}Mg_{0.07}Ca_{0.05})^{2+}(Fe_{3.91})^{3+}(SO_4)_6(OH)_2 \cdot 20H_2O$	0.20	0.12	0.11
Voltaite, IMJ-05: $(K_{1.12}Na_{0.05})^{+}(Fe_{3.45}Mg_{1.17}Ca_{0.09}Zn_{0.06}Mn_{0.06}Cu_{0.05})^{2+}$ $(Fe_{2.85}Al_{1.0}B_{0.01})^{3+}(SO_4)_{12} \cdot 18H_2O$	0.56	0.55	0.56
Voltaite, IM-06: $(K_{1.48}Na_{0.06})^{+}(Fe_{3.40}Mg_{0.82}Zn_{0.71}Cu_{0.11}Ca_{0.06}Cd_{0.01})^{2+}$ $(Fe_{3.13}Al_{1.03})^{3+}(SO_4)_{12} \cdot 18H_2O$	0.56	0.52	
Voltaite, IMJ-06: $(K_{1.4}Na_{0.05})^{+}(Fe_{3.79}Mg_{0.53}Zn_{0.42}Cu_{0.13}Ca_{0.09}Cd_{0.01}Mn_{0.01})^{2+}$ $(Fe_{2.79}Al_{0.91})^{3+}(SO_4)_{12} \cdot 18H_2O$	0.56	0.60	0.58
Kornelite, IM-09: $(Fe_{1.85})^{3+}(SO_4)_3 \cdot 7H_2O$	0.00	0.00	
Römerite, IM-10: $(Fe_{0.80}Zn_{0.16}Mg_{0.02})^{2+}(Fe_{1.94}Al_{0.01})^{3+}(SO_4)_4 \cdot 14H_2O$	0.33	0.29	0.29
Coquimbite, IM-12: $(Fe_{1.73}Al_{0.21})^{3+}(SO_4)_3 \cdot 9H_2O$	0.00	0.00	
Rozenite, IM-13: $(Fe_{0.91}Zn_{0.03}Mg_{0.01})^{2+}SO_4 \cdot 4H_2O$	1.00	1.00	
Siderotil, IM-14: $(Fe_{0.57}Cu_{0.22}Zn_{0.13}Mg_{0.02})^{2+}SO_4 \cdot 5H_2O$	1.00	1.00	
Synthetic samples			
Ferricopiapite: $Fe^{3+}_{4.78}(SO_4)_6(OH)_2 \cdot 20H_2O$	1.00	1.00	
$Fe_2(SO_4)_3$ (monoclinic): $Fe_{2.00}(SO_4)_3$	1.00	1.00	
$Fe_2(SO_4)_3 \cdot 5H_2O$: $Fe^{3+}_{2.1}(SO_4)_3 \cdot 5H_2O$	1.00	1.00	
Hydronium jarosite: $(H_3O)_{0.91}Fe_{2.91}(SO_4)_2[(OH)_{5.64}(H_2O)_{0.18}]$	1.00	1.00	
Rhomboclase: $(H_3O)Fe^{3+}_{0.92}(SO_4)_2 \cdot 3H_2O$	1.00	1.00	

[a] derived from chemical analyses.
[b] derived from Mössbauer data. Uncertainty on the areas of the components is better than 2%.

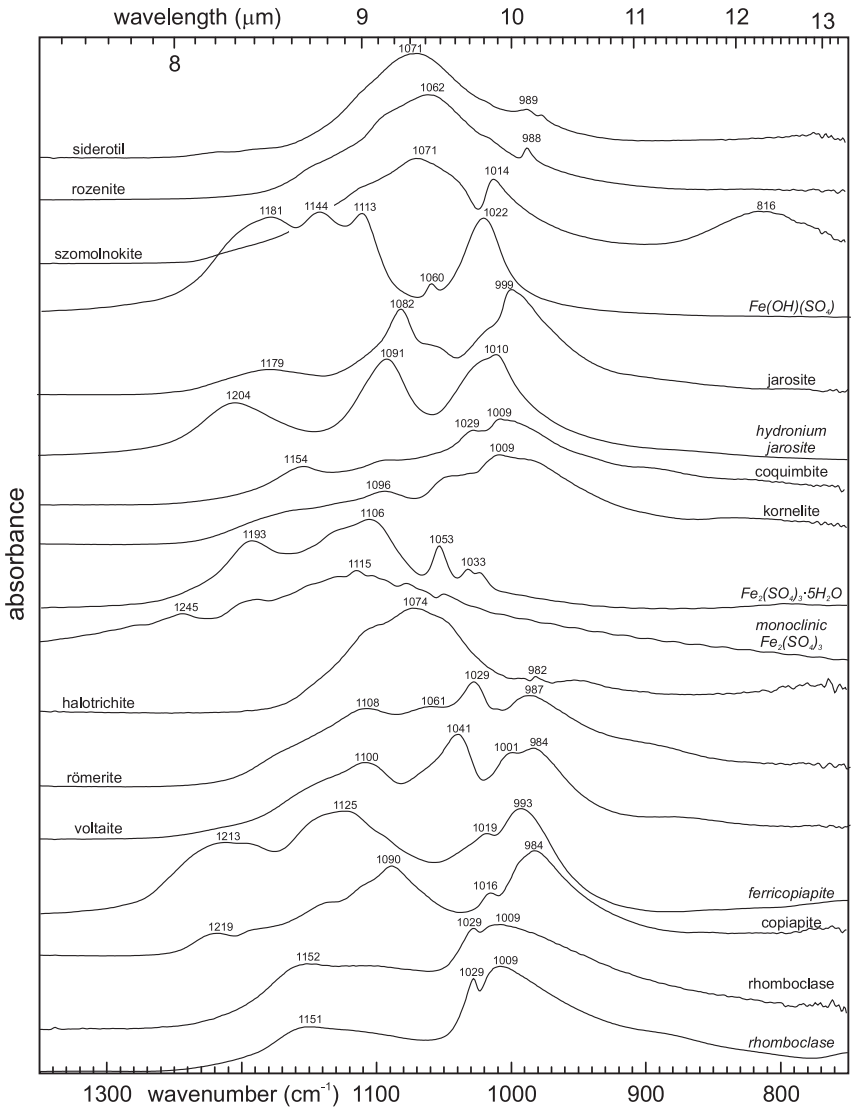

Fig. 2. FTIR spectra in the region 750–1350 cm^{-1}. Names or formulae of the synthetic samples are given in italics.

(Table 1). The ν_1SO_4 band is resolved in all spectra (Fig. 2). The remaining three ν_3SO_4 bands overlap in a broad band centered at 1062–1071 cm^{-1}. From this group of minerals, only melanterite has been studied in some detail (Gamo, 1961; Reddy et al., 2001) so its spectrum is not reported here. The spectrum of szomolnokite is distinguished from the other ferrous sulfate hydrates by a broad feature at ~816 cm^{-1}, a distinctly different position of the ν_1SO_4 band, and a weak peak at 1490 cm^{-1}. Similar features were also observed in spectra of szomolnokite by Cody and Biggs (1973) and Adler and Kerr (1965).

4.2.2. Jarosite group and Fe(OH)(SO4)

Compounds isostructural with jarosite have the general formula $AB_3(SO_4)_2(OH)_6$, where $A = K^+$, Na^+, and H_3O^+ and $B = Fe^{3+}$ and Al^{3+} (Stoffregen et al., 2000); other cations are much less common. These compounds frequently contain H_2O molecules that compensate for deficiency on *B* site. The single sulfur site has C_{3v} symmetry. Therefore, the spectra (Fig. 2) should show 3 sulfate bands ($2\,\nu_3SO_4 + \nu_1SO_4$), δOH, νOH, and weak water bands. Vibrational spectra of jarosite-type compounds were investigated in detail by Serna et al. (1986) and Breitinger et al. (1997) who performed a complete group-factor analysis. Powers et al. (1975) investigated a series of jarosite, deuterated jarosite, chromate analog of jarosite, and deuterated chromate jarosite in order to separate individual bands. Infrared and visible spectra of jarosite and alunite compounds were re-investigated in detail by Bishop and Murad (2005). The ν_1SO4 band occurs at 1000–1015 cm^{-1}, and the ν_3SO_4 bands at 1075–1095 and 1185–1205 cm^{-1}. The δOH band overlaps with ν_1SO4 band and was reported at 1000–1030 cm^{-1}. The weak ν_2w band is located at 1630–1640 cm^{-1} (Fig. 3). The high-frequency region (2900–3660 cm^{-1}, Fig. 3) contains the νOH stretching bands. FTIR spectra of Ag^+, K^+, and NH_4^+ jarosite (Sasaki and Konno, 2000) and biological and inorganic jarosite (Tuovinen and Carlson, 1979) differ only in minor details from those presented in this work.

The IR spectrum of Fe(OH)(SO_4) (Figs. 2, 3) was investigated by Powers et al. (1975). This compound contains a single sulfur site with site symmetry C_s. Powers et al. (1975) located the 4 expected sulfate bands at 1172, 1138, 1112, and 1058 cm^{-1}. The δOH band occurs at 1020 and the νOH band at 3458 cm^{-1}.

4.2.3. Ferric sulfate hydrates

Among the minerals with the general formula $Fe_2(SO_4)_3 \cdot nH_2O$, only coquimbite is relatively common. Monoclinic $Fe_2(SO_4)_3$ is not known from nature, however, the trigonal polymorph was described from a single occurrence and named mikasaite (Miura et al., 1994). Because of their rarity, there are essentially no spectroscopic data for these minerals. All of them have low symmetries at sulfur sites, and therefore 4 sulfate bands are expected for each sulfate site. The

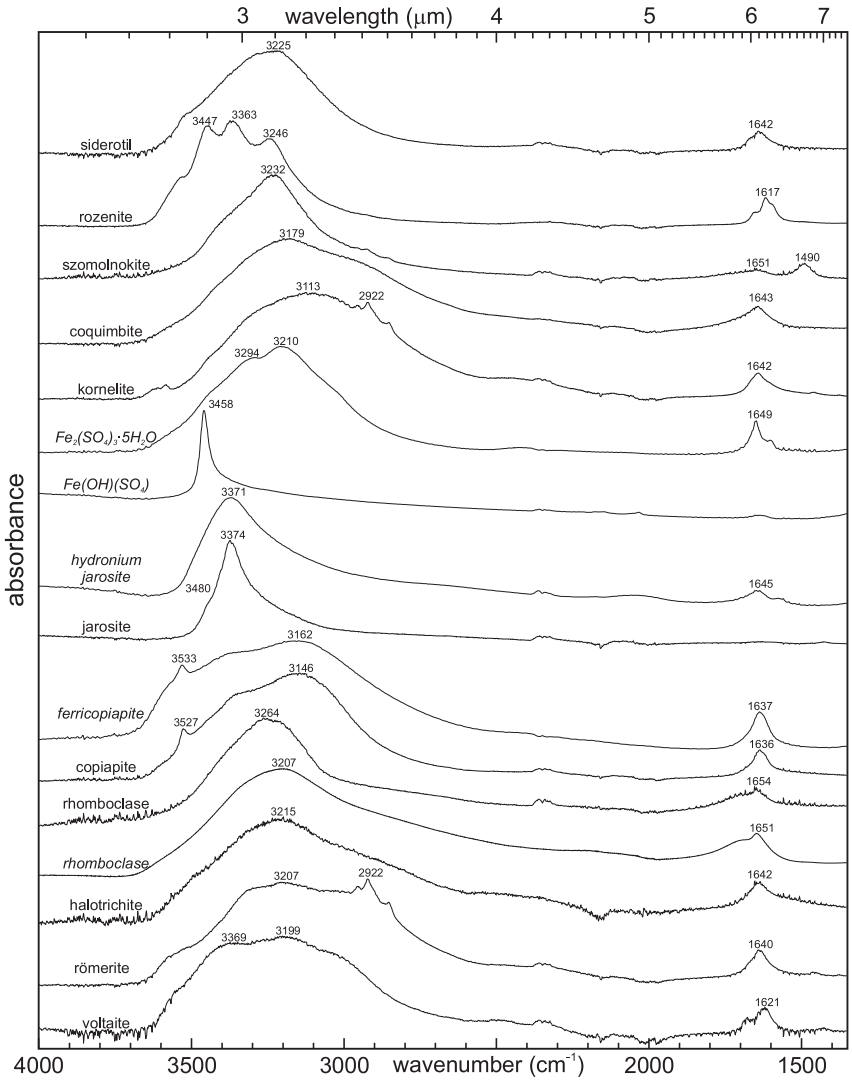

Fig. 3. FTIR spectra in the region 1350–4000 cm^{-1}. Names of the synthetic samples are given in italics. In the spectra of kornelite and romerite, the triplet with a peak at 2922 cm^{-1} is characteristic of the C—H stretching vibrations, not O—H stretches, probably from an organic impurity. The weak bands at ~1450 cm^{-1} are due to the C—H bending vibrations.

spectra of monoclinic $Fe_2(SO_4)_3$ and $Fe_2(SO_4)_3 \cdot 5H_2O$ (Fig. 2) show bands centered at ~1100 cm^{-1}. The spectra of higher hydrates (Fig. 2) show the center of the sulfate bands at somewhat lower frequencies.

4.2.4. Rhomboclase and copiapite

The compounds isostructural with rhomboclase have the general formula $(H_5O_2)A(SO_4)_2 \cdot 2H_2O$ where $A = Fe^{3+}$, In^{3+}, and Tl^{3+} (Brach and Goodenough, 1988). Rhomboclase should show 4 sulfate bands in the investigated spectral range. However, the mobility of one of the structural protons (Brach and Goodenough, 1988) may introduce variations in the local environment of the sulfate ion and complicate the spectral analysis. The spectra of natural and synthetic rhomboclase are very similar (Figs. 2 and 3), indicating that the chemical composition of this compound is rather constant and very little substitution, except for rare Tl and In, is possible. The broad shoulder below 900 cm^{-1} in the spectrum of synthetic rhomboclase coincides with the S—OH stretching mode of the bisulfate ion at 890 cm^{-1}, and perhaps points at the possibility of sulfate ion protonation.

The copiapite group has the general formula $A{Fe^{3+}}_4(SO_4)_6(OH)_2 \cdot 20H_2O$ where $A = Fe^{2+}$, Mg^{2+}, Zn^{2+}, Ca^{2+}, Cu^{2+}, Co^{2+}, Mn^{2+}, Ni^{2+}, $2/3Fe^{3+}$, or $2/3Al^{3+}$ (Atencio et al., 1996). Three sulfate sites, each with C_1 symmetry (Table 1), correspond to 12 sulfate bands in addition to M—O—H bands in the low-frequency part of the spectra (Fig. 2). The large number of overlapping bands precludes their separation and the reliable identification of sulfate and hydroxyl vibrations. A common feature of both natural copiapite and synthetic ferricopiapite is a distinctly sharp νOH band at ~3530 cm^{-1} (Fig. 3).

4.2.5. Halotrichite, voltaite, and römerite

These three minerals are not well studied by IR and Raman spectroscopy. Halotrichite belongs to a group of pseudo-alums, with

Table 4
Vibrational modes for group SO_4.

Site symmetry	Γ_{vib}
C_1	$9A^{IR,R}$
C_2	$5A^{IR,R} + 4B^{IR,R}$
C_3	$3A^{IR,R} + 3E^{IR,R}$
C_s	$6A'^{IR,R} + 3A''^{IR,R}$
C_{2v}	$4A_1^{IR,R} + A2^R + 2B_1^{IR,R} + 2B_2^{IR,R}$
C_{3v}	$3A_1^{IR,R} + 3E^{IR,R}$
D_2	$3A^R + 2B_1^{IR,R} + 2B_2^{IR,R} + 2B_3^{IR,R}$
D_{2d}	$2A_1^R + B_1^R + 2B_2^{IR,R} + 2E^{IR,R}$
S_4	$2A^R + 3B^{IR,R} + 2E^{IR,R}$
T	$A^R + E^R + 2T^{IR,R}$
T_d	$A_1^R + E^R + 2T_2^{IR}$

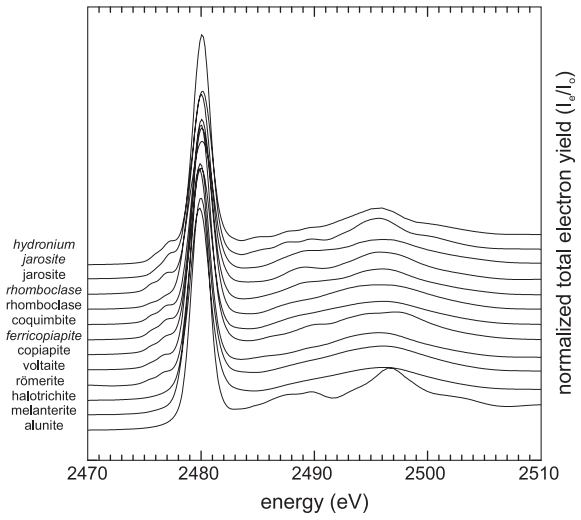

Fig. 4. XANES spectra of the studied sulfates. Names of the synthetic samples are given in italics.

the general formula $AAl_2(SO_4)_3 \cdot 22H_2O$ where $A = Fe^{2+}$. The other two common phases are pickeringite ($A = Mg^{2+}$), and apjohnite ($A = Mn^{2+}$). The only detailed vibrational spectroscopic investigation on these minerals was a Raman study of halotrichite and apjohnite (Frost et al., 2000). Frost et al. (2000) assigned the 982 cm^{-1} band (Fig. 2) and a weaker band at 995 cm^{-1} (not present in our IR spectrum) in halotrichite to the $\nu_1 SO_4$ vibrations for the sulfate bonded to Fe^{2+} octahedron and a hydrogen-bonded sulfate ion, respectively. A weak and broad band at 955 cm^{-1} was assigned to water librational modes (Ross, 1974; Frost et al., 2000). The remaining halotrichite sulfate IR bands are overlapping and contributing to a broad band centered at 1074 cm^{-1}. In this study's IR spectrum of römerite, the $\nu_1 SO_4$ band is clearly resolved at 987 cm^{-1}, and the bands of the spectrum do not correspond to the positions of bands in a römerite spectrum reported by Ross (1974).

4.3. XANES spectroscopy

X-ray absorption spectroscopy measures the transitions of core electrons into outer bound or unbound states (Brown and Sturchio, 2002). These transitions are possible only when the incident radiation has a sufficient energy to transfer core electrons into a free electron state. At that energy, absorption of the sample rises, and the energy region is called the absorption edge. This region is of interest in X-ray absorption near-edge spectroscopy (XANES). The position of the absorption edge is element specific and depends on the shell from which the electrons are ejected. In addition, the position of the absorption edge varies slightly with oxidation state of the element, e.g., by more than 10 eV for sulfur (Pickering et al., 1998). Variations in the shape of the absorption peak can be related to the element's local environment. Myneni (2000) described the experimental setup and the facilities for collecting sulfur XANES spectra.

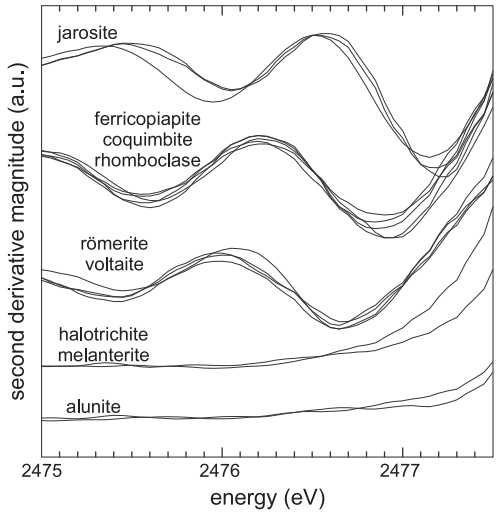

Fig. 5. Second derivative of the pre-edge region in the XANES spectra of the studied sulfates.

At the sulfur K edge, the XANES spectra of our samples show a sharp peak at ~2480 eV and broader post-edge features (Fig. 4). The peak was attributed to $1s \rightarrow t_2$ transitions, and the post-edge features to transitions of 1*s* electrons into unbound states (Myneni, 2000). The position of the main peak shows a little variability and lies between 2479.9 and 2480.1 eV, and its full width at half maximum (FWHM) is 1.9–2.3 eV. For comparison, the position of the main peak for aqueous sulfate and bisulfate is 2479.7 and 2479.8 eV, respectively. The FWHM for aqueous sulfate and bisulfate is 1.7 and 2.1 eV, respectively.

Weak pre-edge features appear in spectra of some of the phases, as also reported by Figueiredo and da Silva (2009). There are no such features in the spectra of alunite ($KAl_3(SO_4)_2(OH)_6$), a sulfate mineral that contains no iron. Similarly, no pre-edge features are found in the spectra of $(NH_4)Fe^{3+}(SO_4)_2 \cdot 12H_2O$ (Myneni, 2000). In this phase, iron octahedra and sulfur tetrahedra are connected exclusively by a hydrogen-bonded network. Pre-edge features are seen in the spectra of those Fe^{3+} sulfates where the iron and sulfur ions are connected by a bridging oxygen (Table 1), that is, they occur in proximity. The pre-edge features originate from the transition of electrons from hybridized S 3*p* states into the 3*d* states of the ferric iron (Okude et al., 1999). Similar pre-edge features appear in P XANES spectra of $Fe_4(PO_4)_3(OH)_3$ (Okude et al., 1999) and Cl XANES spectra of $FeCl_3 \cdot 6H_2O$ (Myneni, 2002).

The position of the pre-edge features is solely a function of the number of bridging oxygens between iron and sulfur as shown by the differences in the second derivative spectra (Fig. 5). Fragments of crystal structures which display the connectivity of iron octahedra and sulfate tetrahedra are shown in Table 1. In jarosite, iron and sulfur share three oxygens; in copiapite, coquimbite, and rhomboclase, two oxygens; and in quenstedtite, voltaite, and römerite, only one oxygen (Table 1). There is no Fe^{3+} in melanterite, halotrichite, and alunite, and no pre-edge features are visible in the spectra of these minerals (Fig. 5) The position of the pre-edge feature is not affected by variations in chemical composition, such as K^+ versus H_3O^+ ions in the interlayer of jarosite, or chemical variability of copiapite samples (Fig. 5).

Because the position of the pre-edge features appears to be fixed by the number of shared oxygen atoms, this position has a potential to serve as an indicator of iron(III) and sulfur connectivity in poorly crystalline, liquid, or bioinorganic samples. The pre-edge features are located at 2477.4 eV for three shared oxygen atoms in the jarosite spectrum, at 2477.0 eV for two shared oxygen atoms in ferricopiapite, and at 2476.8 eV of one shared oxygen atom in römerite (Fig. 5).

4.4. Mössbauer spectroscopy

Mössbauer spectroscopy probes the nuclear transition in a suitable isotope, and is sensitive to the geometry of the electronic environment around the probed atoms. ^{57}Fe is the most widely used Mössbauer isotope, and the transition observed is the 3/2 → 1/2 transition at 14.4 keV (McCammon, 1995). Mössbauer spectroscopy can successfully differentiate oxidation states and local coordination of ^{57}Fe in a variety of geological materials (Hawthorne, 1988; McCammon, 1995). The relevant data extracted from the fitting procedure of spectra collected at 80 K are summarized in Table 5.

Table 5
Mössbauer parameters for octahedrally coordinated Fe in the studied sulfate minerals at 80 K. δ is the isomer shift, ΔE_Q is the quadrupole splitting, Γ is the line width, and A is the spectral area.

Phase, sample ID	Fe(III)				Fe(II)			
	δ (mms^{-1})	ΔE_Q (mms^{-1})	Γ (mms^{-1})	A (%)	δ (mms^{-1})	ΔE_Q (mms^{-1})	Γ (mms^{-1})	A (%)
Jarosite, IMJ-09	0.49	1.24	0.36	100				
Rhomboclase, IM-02	0.54	0.59	0.27	100				
Copiapite, IM-05	0.53	0.80	0.26	44	1.38	3.19	0.25	11
	0.53	0.38	0.26	45				
Copiapite, 91RS210A	0.53	0.79	0.34	54	1.35	3.11	0.40	4
	0.53	0.30	0.31	42				
Römerite, IM-10	0.52	0.38	0.63	56	1.38	3.49	0.30	29
	0.59	0.17	0.50	15				
Voltaite, IMJ-05	0.59	0.26	0.36	44	1.42	2.69	0.45	56
Voltaite, 91RS210A	0.59	0.26	0.36	45	1.42	2.68	0.46	55
Voltaite, IMJ-06	0.59	0.27	0.35	42	1.41	2.96	0.29	21
					1.41	2.52	0.42	37

Uncertainties are better than 0.05 mms^{-1} and areas better than 2%.

4.4.1. Jarosite group

The Mössbauer spectrum of natural jarosite (Fig. 6) exhibits a characteristic ferric doublet with a high quadrupole splitting (Table 5). This large quadrupole splitting may indicate that the local environment around Fe^{3+} is highly distorted and is in a good agreement with previously published values (Johnston, 1977; Leclerc, 1980).

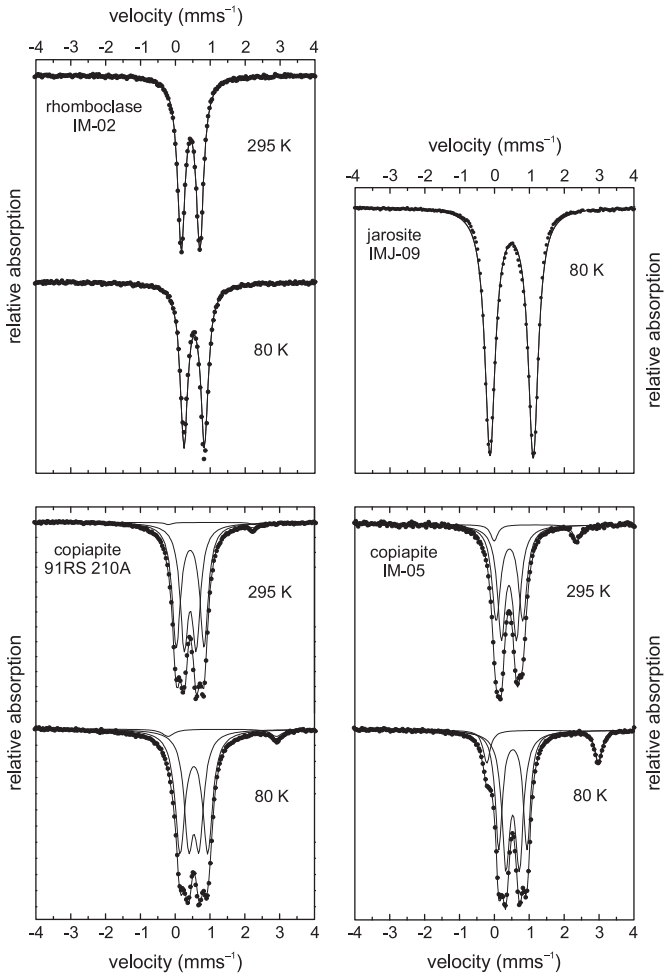

Fig. 6. Mössbauer spectra of jarosite, copiapite, and rhomboclase.

4.4.2. Rhomboclase and copiapite

The Mössbauer spectrum of natural rhomboclase (Fig. 6) exhibits a simple ferric high-spin doublet (isomer shifts 0.43 and 0.54 mm s^{-1} and quadrupole splittings 0.53 and 0.59 mm s^{-1} at RT and 80 K, respectively). These parameters are very similar to those for a synthetic sample that exhibits magnetic ordering between 20 and 5 K (spectra not shown here). The asymmetry observed in the spectrum measured at 80 K is due to a texture effect that is eliminated in the spectrum measured at RT and at the magic angle of 54.7°. No signal attributable to ferrous iron can be discerned from the spectrum of rhomboclase.

Copiapite exhibits a complex Mössbauer spectrum with individual components resolved at 80 K (Fig. 6). The spectrum is dominated by ferric components with a minor ferrous contribution (all high spin state). Two ferric components are resolved in the spectrum and their Mössbauer parameters are listed in Table 5. The parameters and relative abundance are very similar to a synthetic ferricopiapite (not shown). The two ferric sites in copiapite correspond to two crystallographic positions for $^{VI}Fe^{3+}$ in agreement with the structural model of Fanfani et al. (1973). The ferrous component has a relative intensity of 11.0% at 80 K. Assuming identical f-factors for all the sites, the relative spectral area can be converted straight-forwardly to a relative amount of ferrous iron in the sample (Table 3).

4.4.3. Voltaite and römerite

The römerite Mössbauer spectra (Fig. 7) contain both ferrous and ferric high-spin components. The ferrous component has an intensity that is close to the ideal (33%) for one ferrous atom per unit cell (Table 5). The ferric component is very broad, making a unique solution to the fitting problem difficult. Fits using two ferric components (Table 5) are satisfactory but not unique. The broadening of the ferric component may be caused by variations in the local coordination. It is interesting to compare the Mössbauer data to the structural information (Table 1). Both techniques indicate a single site for ferrous iron.

Both ferrous and ferric components in the Mössbauer spectra of the voltaite samples (Fig. 7 and Table 5) are high spin and are dominated by the ferrous components. The resolution of the spectrum increases on lowering the temperature due to the stronger temperature dependence of the splitting of the ferrous lines. We note the slightly increased line width also of the ferrous component probably indicating some variation in local coordination. The Mössbauer parameters for all voltaite samples are very similar and only those for two samples are given in Table 5. In addition, a minor ferrous component in the sample IMJ-06 has an isomer shift of 1.40 mm s^{-1} and a quadrupole splitting of 2.99 mm s^{-1}. Such a component has not been reported from other voltaite samples.

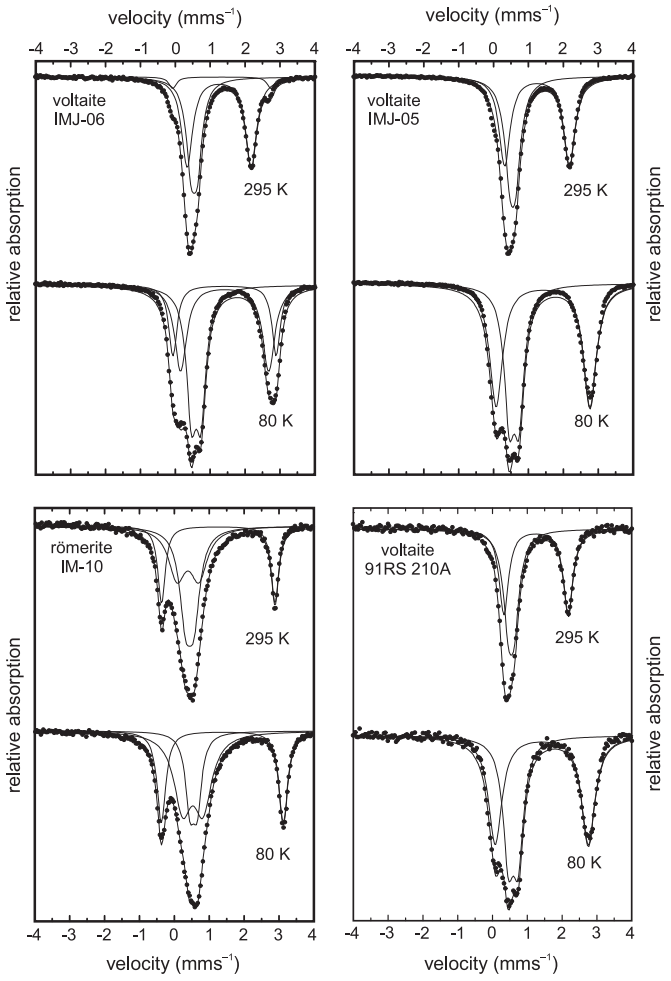

Fig. 7. Mössbauer spectra of voltaite and römerite.

5. Concluding remarks

We reported and described infrared, X-ray absorption, and Mössbauer spectra for a suite of iron-sulfate minerals and related phases. The spectral features (positions of IR bands, positions of pre-edge features, and hyperfine parameters) are in a good agreement with the structural details deduced from the structural models of the studied phases. Although the agreement is not perfect and the interpretation of the spectra is not always unequivocal, the presented spectra can be used for identification of the sulfate minerals or description of processes which involve the interaction of iron and sulfate.

In particular, the infrared and Mössbauer data can be helpful for the identification of the materials on Mars, and possibly on other bodies, from the planetary missions data (cf. Bishop et al. (2005), Lane et al. (2008)). Although the spectral resolution of the instruments on these missions is usually lower than that achieved in the terrestrial laboratories, our spectra provide a good framework for the evaluation of the missions data. Furthermore, our spectra can be compared to the results of others (Lane et al., 2004; Cloutis et al., 2006; Lane, 2007) who used natural or synthetic samples in their studies. The differences in the spectra can then indicate the possible variations within a single mineral species or among different procedures employed to collect the data.

The X-ray absorption data can be used where the standard (e.g., single-crystal studies, Rietveld refinement of powder data) or advanced (e.g. pair-distribution function) crystallographic techniques come short of or fail to give a satisfactory answer about the bonding environment of sulfate in a given sample. These may include crystals where the local structure deviates significantly from the "average" one, poorly-crystalline materials, nanomaterials, and aqueous and non-aqueous liquids (e.g., Waychunas et al., 2001; Majzlan and Myneni, 2005).

Acknowledgments

We thank D. Dingwell for the editorial handling of the manuscript and an anonymous reviewer for helpful comments. Samples from Iron Mountain were collected with the cooperation of the U.S. Environmental Protection Agency. We appreciate the help of beamline scientists B. Hedman and G.N. George at the Stanford Synchrotron Radiation Lightsource.

References

Adler, H.H., Kerr, P.F., 1965. Variations in infrared spectra molecular symmetry and site symmetry of sulfate minerals. American Mineralogist 50, 132–147.
Alpers, C.N., Nordstrom, D.K., Spitzley, J., 2003. Extreme acid mine drainage from a pyritic massive sulfide deposit: the Iron Mountain end-member. In: Jambor, J.L., Blowes, D.W., Ritchie, A.I.M. (Eds.), Environmental Aspects of Mine Wastes, vol. 31. Mineralogical Association of Canada, Short-Course, pp. 407–430.
Atencio, D., Carvalho, F.M.S., Hypolito, R., 1996. Synthesis and X-ray powder diffraction data for Mg-, Al- and Ni- end-members of the copiapite group. Anais Assoc. Brais. Quím 45, 66–72.
Baur, W.H., 1962. Zur Kristallchemie der Salzhydrate. Die Kristallstrukturen von $MgSO_4(H_2O)_4$ (Leonhardtit) und $FeSO_4(H_2O)_4$ (Rozenit). Acta Crystallographica 15, 815–826.
Bishop, J.L., Dyar, M.D., Lane, M.D., Banfield, J., 2005. Spectral identification of hydrated sulfates on Mars and comparison with acidic environments on Earth. International Journal of Astrobiology 3, 275–285.
Bishop, J.L., Murad, E., 2005. The visible and infrared spectral properties of jarosite and alunite. American Mineralogist 90, 1100–1107.
Brach, I., Goodenough, J.B., 1988. Influence of the M(III) cation on proton conduction in rhomboclases. Solid State Ionics 27, 243–249.
Breitinger, D.K., Krieglstein, R., Bogner, A., Schwab, R.G., Pimpl, Th.H., Mohr, J., Schukow, H., 1997. Vibrational spectra of synthetic minerals of the alunite and crandallite type. Journal of Molecular Structure 408 (409), 287–290.
Brown Jr., G.E., Sturchio, N.C., 2002. An overview of synchrotron radiation applications to low temperature geochemistry and environmental science. In: Fenter, P.A., Rivers, M.L., Sturchio, N.C., Sutton, S.R. (Eds.), Applications of Synchrotron Radiation in Low-temperature Geochemistry and Environmental Science: Reviews in Mineralogy and Geochemistry, 49, pp. 1–115.
Buckby, T., Black, S., Coleman, M.L., Hodson, M.E., 2003. Fe-sulphate-rich evaporative mineral precipitates from the Rio Tinto, southwest Spain. Mineralogical Magazine 67, 263–278.
Cloutis, E.A., Hawthorne, F.C., Mertzman, S.A., Krenn, K., Craig, M.A., Marcino, D., Methot, M., Strong, J., Mustard, J.F., Blaney, D.L., Bell III, J.F., Vilas, F., 2006. Detection and discrimination of sulfate minerals using reflectance spectroscopy. Icarus 184, 121–157.
Cody, R.D., Biggs, D.L., 1973. Halotrichite, szomolnokite, and rozenite from Dolliver State Park, Iowa. Canadian Mineralogist 11, 958–970.
Dyar, M.D., Lane, M.D., Bishop, J.L., O'Connor, V., Cloutis, E., Hiroi, T., 2005. Integrated spectroscopic studies of hydrous sulfate minerals. 36th Lunar and Planetary Science Conference. Abstracts.
Fanfani, L., Nunzi, A., Zanazzi, P.F., 1970. The crystal structure of roemerite. American Mineralogist 55, 78–89.
Fanfani, L., Nunzi, A., Zanazzi, P.F., Zanzari, A.R., 1973. Copiapite problem — crystal-structure of a ferrian copiapite. American Mineralogist 58, 314–322.
Fang, J.H., Robinson, P.D., 1970. Crystal structures and mineral chemistry of hydrated ferric sulfates. I. Crystal structure of coquimbite. American Mineralogist 55, 1534–1540.
Farmer, V.C. (Ed.), 1974. The Infrared Spectra of Minerals: Mineralogical Society Monograph, 4, pp. 423–444.
Figueiredo, M.O., da Silva, T.P., 2009. Effect of oxygen sharing on the white line of S K-edge XANES spectra of sulphate minerals. European Journal of Mineralogy 21, 79–83.
Frost, R.L., Kloprogge, J.T., Williams, P.A., Leverett, P., 2000. Raman microscopy of some natural pseudo-alums: halotrichite, apjohnite and wupatkiite, at 298 and 77 K. Journal of Raman Spectroscopy 31, 1083–1087.
Gamo, I., 1961. Bandes d'absorption infrarouges dues a lion SO_4 dans $NiSO_4.7H_2O$, $FeSO_4.7H_2O$, $CoSO_4.7H_2O$ et $MgSO_4.7H_2O$. Comptes Rendus Hebdomadaires des Seances de l'Academie des Sciences 253, 1429–1431.
Geissler, P.E., Singer, R.B., Komatsu, G., Murchie, S., Mustard, J., 1993. An unusual spectral unit in West Candor chasma: evidence for aqueous or hydrothermal alteration in the Martian canyons. Icarus 106, 380–391.
Gendrin, A., Mangold, N., Bibring, J.P., Langevin, Y., Gondet, B., Poulet, F., Bonello, G., Quantin, C., Mustard, J., Arvidson, R., LeMouelic, S., 2005. Sulfates in Martian layered terrains: the OMEGA/Mars Express view. Science 307, 1587–1591.
Harris, D.C., Bertolucci, M.D., 1978. Symmetry and spectroscopy. An Introduction to Vibrational and Electronic Spectroscopy. Dover Publications, Inc, New York. 550 pp.

Hawthorne, F.C., 1988. Mössbauer spectroscopy. In: Hawthorne, F.C. (Ed.), Spectroscopic Methods in Mineralogy and Geology: Reviews in Mineralogy, pp. 255–340.
Hawthorne, F.C., Krivovichev, S.V., Burns, P.C., 2000. The crystal chemistry of sulfate minerals. In: Alpers, C.N., Jambor, J.L., Nordstrom, D.K. (Eds.), Sulfate Minerals — Crystallography, Geochemistry, and Environmental Significance: Reviews in Mineralogy and Geochemistry, 40, pp. 1–112.
Hendricks, S.B., 1937. The crystal structure of alunite and the jarosites. American Mineralogist 22, 773–784.
Hunt, G.R., 1979. Near-infrared (1.3–2.4 μm) spectra of alteration minerals — potential for use in remote sensing. Geophysics 44, 1974–1986.
Jambor, J.L., Nordstrom, D.K., Alpers, C.N., 2000. Metal–sulfate salts from sulfide mineral oxidation. In: Alpers, C.N., Jambor, J.L., Nordstrom, D.K. (Eds.), Sulfate Minerals — Crystallography, Geochemistry, and Environmental Significance: Reviews in Mineralogy and Geochemistry, 40, pp. 303–350.
Johansson, G., 1962. On the crystal structure of $FeOHSO_4$ and $InOHSO_4$. Acta Chemica Scandinavica 16, 1234–1244.
Johnston, J.H., 1977. Jarosite and akaganeite from White Island volcano, New Zealand — an X-ray and Mössbauer study. Geochimica et Cosmochimica Acta 41, 539–544.
Klingelhöfer, G., Morris, R.V., Bernhardt, B., Schroder, C., Rodionov, D.S., de Souza, P.A., Yen, A., Gellert, R., Evlanov, E.N., Zubkov, B., Foh, J., Bonnes, U., Kankeleit, E., Gutlich, P., Ming, D.W., Renz, F., Wdowiak, T., Squyres, S.W., Arvidson, R.E., 2004. Jarosite and hematite at Meridiani Planum from Opportunity's Mössbauer spectrometer. Science 306, 1740–1745.
Langevin, Y., Poulet, P., Bibring, J.-P., Gondet, B., 2005. Sulfates in the north polar region of Mars detected by OMEGA/Mars Express. Science 307, 1584–1586.
Lane, M.D., 2007. Mid-infrared emission spectroscopy of sulfate and sulfate-bearing minerals. American Mineralogist 92, 1–18.
Lane, M.D., Bishop, J.L., Dyar, M.D., King, P.L., Parente, M., Hyde, B.C., 2008. Mineralogy of the Paso Robles soils on Mars. American Mineralogist 93, 728–739.
Lane, M.D., Dyar, M.D., Bishop, J.L., 2004. Spectroscopic evidence for hydrous iron sulfate in the Martian soil. Geophysical Research Letters 31. doi:10.1029/2004GL021231.
Larson, A.C., von Dreele, R.B., 1994. GSAS. General Structure Analysis System. LANSCE, MS-H805, Los Alamos, New Mexico.
Leclerc, A., 1980. Room-temperature Mössbauer analysis of jarosite-type compounds. Physics and Chemistry of Minerals 6, 327–334.
le Fur, Y., Coing-Boyat, J., Bassi, G., 1966. Structure des sulfates monohydrates, monocliniques, des metaux de transition, $MSO_4(H_2O)$ (M = Mn, Fe, Co, Ni et Zn). Comptes Rendus Hebdomadaires des Seances de l'Academie des Sciences, Serie C, Sciences Chimiques 262, 632–635.
Long, G.J., Longworth, G., Battle, P., Cheetham, A.K., Thundathil, R.V., Beveridge, D., 1979. A study of anhydrous iron(III) sulfate by magnetic susceptibility, Mossbauer, and neutron diffraction techniques. Inorganic Chemistry 18, 624–632.
Majzlan, J., Botez, C., Stephens, P.W., 2005. The crystal structures of $Fe_2(SO_4)_3(H_2O)_5$ and the type specimen of lausenite. American Mineralogist 90, 411–416.
Majzlan, J., Michallik, R., 2007. The crystal structures, solid solutions and infrared spectra of copiapite-group minerals. Mineralogical Magazine 71, 557–573.
Majzlan, J., Myneni, S.C.B., 2005. Speciation of iron and sulfate in acid waters: aqueous clusters to mineral precipitates. Environmental Science & Technology 39, 188–194.
McCammon, C., 1995. Mössbauer spectroscopy of minerals. Mineral physics and crystallography, A Handbook of physical constants. AGU Reference Shelf 2, 332–347.
Mereiter, K., 1972. Die Kristallstruktur des Voltaits, $K_2Fe^{2+}{}_5Fe^{3+}{}_3Al[SO_4]_{12}\cdot 18H_2O$. Tschermaks Mineralogische und Petrographische Mitteilungen 18, 185–202.
Mereiter, K., 1974. Die Kristallstruktur von Rhomboklas $(H_5O_2)^+(Fe(SO_4)_2(H_2O)_2)$. Tschermaks Mineralogische und Petrographische Mitteilungen 21, 216–232.
Miura, H., Niida, K., Hirama, T., 1994. Mikasaite, $(Fe^{3+}, Al)_2(SO_4)_3$, a new ferric sulphate mineral from Mikasa City, Hokkaido, Japan. Mineralogical Magazine 58, 649–653.
Montero-Sanchez, I.C., Brimhall, G.H., Alpers, C.N., Swayze, G.A., 2005. Characterization of waste rock associated with acid drainage at the Penn Mine, California by ground-based visible to short-wave infrared reflectance spectroscopy assisted by digital mapping. Chemical Geology 215, 453–472.
Morris, R.V., Klingenhöfer, G., Bernhardt, B., Schroder, C., Rodionov, D.S., de Souza, P.A., Yen, A., Gellert, R., Evlanov, E.N., Foh, J., Kankeleit, E., Gutlich, P., Ming, D.W., Renz, F., Wdowiak, T., Squyres, S.W., Arvidson, R.E., 2004. Mineralogy at Gusev Crater from the Mössbauer spectrometer on the Spirit Rover. Science 305, 833–836.
Myneni, S.C.B., 2000. X-ray and vibrational spectroscopy of sulfate in Earth materials. In: Alpers, C.N., Jambor, J.L., Nordstrom, D.K. (Eds.), Sulfate Minerals. Crystallography, Geochemistry, and Environmental Significance: Reviews in Mineralogy and Geochemistry, 40, pp. 113–172.
Myneni, S.C.B., 2002. Formation of stable chlorinated hydrocarbons in weathering plant material. Science 295, 1039–1041.
Nielsen, U.G., Majzlan, J., Grey, C.P., 2008. Identification of local environments in defect jarosite ($AFe_3(SO_4)_2(OD)_6$, $A = D_3O$, Na, K) samples by ^2H MAS NMR spectroscopy. Chemistry of Materials 20, 2234–2241.
Nordstrom, D.K., Alpers, C.N., 1999. Negative pH, efflorescent mineralogy, and consequences for environmental restoration at the Iron Mountain Superfund site, California. In: Smith, J.V. (Ed.), Geology, Mineralogy, and Human Welfare: Proceedings of the National Academy of Sciences, USA, 96, pp. 3455–3462.
Nordstrom, D.K., Alpers, C.N., Ptacek, C.J., Blowes, D.W., 2000. Negative pH and extremely acidic mine waters from Iron Mountain, California. Environmental Science & Technology 34, 254–258.
Okude, N., Nagoshi, M., Noro, H., Baba, Y., Ymamoto, H., Sasaki, T.A., 1999. P and S K-edge XANES transition-metal phosphates and sulfates. Journal of Electron Spectroscopy and Related Phenomena 101–103, 607–610.
Peterson, R.C., Roeder, P.L., You-Sheng, Zhang, 2003. The atomic structure of siderotil, $(Fe, Cu)SO_4\cdot 5H_2O$. Canadian Mineralogist 41, 671–676.
Pickering, I.J., Prince, R.C., Divers, T., George, G.N., 1998. Sulfur K-edge X-ray absorption spectroscopy for determining the chemical speciation of sulfur in biological systems. FEBS Letters 441, 11–14.
Posnjak, E., Merwin, H.E., 1922. The system, Fe2O3–SO3–H2O. Journal of the American Chemical Society 44, 1965–1994.
Powers, D.A., Rossman, G.R., Schugar, H.J., Gray, H.B., 1975. Magnetic-behavior and infrared-spectra of jarosite, basic iron sulfate, and their chromate analogs. Journal of Solid State Chemistry 13, 1–13.
Quartieri, S., Triscari, M., Viani, A., 2000. Crystal structure of the hydrated sulphate pickeringite $MgAl_2(SO_4)_4\cdot 22H_2O$: X-ray powder diffraction study. European Journal of Mineralogy 12, 1131–1138.
Reddy, S.N., Rao, P.S., Ravikumar, R.V.S.S.N., Reddy, B.J., Reddy, Y.P., 2001. Spectral investigations on melanterite mineral from France. Spectrochimica Acta A 57, 1283–1287.
Ripmeester, J.A., Ratcliffe, C.I., Dutrizac, J.E., Jambor, J.L., 1986. Hydronium ion in the alunite–jarosite group. Canadian Mineralogist 24, 435–447.
Robinson, P.D., Fang, J.H., 1973. Crystal structures and mineral chemistry of hydrated ferric sulphates. III. The crystal structure of kornelite. American Mineralogist 58, 535–539.
Ross, S.D., 1974. Sulphates and other oxy-anions of Group VI. In: Farmer, V.C. (Ed.), The Infrared Spectra of Minerals: Mineralogical Society Monograph, 4, pp. 423–444.
Ryskin, Ya.I., 1974. The vibrations of protons in minerals: hydroxyl, water, and ammonium. In: Farmer, V.C. (Ed.), The Infrared Spectra of Minerals: Mineralogical Society Monograph, 4, pp. 137–181.
Sasaki, K., Konno, H., 2000. Morphology of jarosite-group compounds precipitated from biologically and chemically oxidized Fe ions. Canadian Mineralogist 38, 45–56.
Serna, C.J., Cortina, C.P., Ramos, J.V.G., 1986. Infrared and Raman study of alunite–jarosite compounds. Spectrochimica Acta 42A, 729–734.
Stoffregen, R.E., Alpers, C.N., Jambor, J.L., 2000. Alunite–jarosite crystallography, thermodynamics, and geochronology. In: Alpers, C.N., Jambor, J.L., Nordstrom, D.K. (Eds.), Sulfate Minerals — Crystallography, Geochemistry, and Environmental Significance: Reviews in Mineralogy and Geochemistry, 40, pp. 453–479.
Stookey, L.L., 1970. Ferrozine — a new spectrophotometric reagent for iron. Analytical Chemistry 42, 779–781.
Swayze, G.A., Smith, K.S., Clark, R.N., Sutley, S.J., Pearson, R.M., Vance, J.S., Hageman, P.L., Briggs, P.H., Meier, A.L., Singleton, M.J., Roth, S., 2000. Using imaging spectroscopy to map acidic mine waste. Environmental Science & Technology 34, 47–54.
Townsend, T.E., 1987. Discrimination of iron alteration minerals in visible and near-infrared reflectance data. Journal of Geophysical Research 92 (B2), 1441–1454.
Tuovinen, O.H., Carlson, L., 1979. Jarosite in cultures of iron-oxidizing Thiobacilii. Journal of Geomicrobiology 1, 205–210.
Vilas, F., Jarvis, K.S., Gaffey, M.J., 1994. Iron alteration minerals in the visible and near-infrared spectra of low-albedo asteroids. Icarus 109, 274–283.
Waychunas, G.A., Myneni, S.C.B., Traina, S.J., Bigham, J.M., Fuller, C.C., Davis, J.A., 2001. Reanalysis of the schwertmannite structure and the incorporation of SO_4^{2-} groups: an IR, XAS, WAXS and simulation study. Abstracts of the 11th Goldschmidt conference.
Wills, A.S., Harrison, A., 1996. Structure and magnetism of hydronium jarosite, a model Kagome antiferromagnet. Journal of the Chemical Society, Faraday Transactions 92, 2161–2166.